Competition sensitive! Draft of 2022.02.05–22:25

Augmenting Lunar Laser Ranging observations with Very Long Baseline Interferometry

Submitted in response to Research Opportunities in Space and Earth Sciences (ROSES) — 2021 Solicitation: NNH21ZDA001N-PDART, program C.4 Planetary Data Archiving, Restoration, and Tools

Contents

1 Executive Summary

We will develop a tool PlaVDA (Planetary VLBI Data Analysis) for processing a Level 1 Very Long Baseline Interferometry (VLBI) data product of Lunar lander observations in a form of a time series of cross- and auto- spectra and generation of a Level 2 data product in a form of differential phase and group delays and delay rates. Availability of that tool will open a window of opportunity for VLBI observations of artificial radio sources placed on the Moon that will augment Lunar Laser Ranging (LLR) observations of retroreflectors delivered to the Moon by prior missions. PlaVDA will be validated using prior VLBI observations of Chang'E3 data in 2015–2016 that are available at the Crustal Dynamics Data Information System (CDDIS) hosted at NASA. Availability of Level 2 VLBI data products will allow to independently check scientific results of LLR and validate them. Combined processing LLR and differential VLBI will improve robustness of scientific results because these two techniques are sensitive to orthogonal projections of instantaneous lander positions.

Processing Level 1 data belongs to a realm of radioastronomy and requires deep knowledge of the VLBI data analysis technique. Users of Level-2 VLBI data are planetary scientists. This projects aims to build a bridge between radioastronomy and planetary science communities.

2 Introduction

Due to the course of the 20th century geodesy evolved from a utilitarian technique for measuring land plots to a foundation of navigation and an environmental science. The Earth surface is static at scales up to several decades at a level of accuracy coarser than 1000 parts per billion (ppb). Measurements with accuracy 100 ppb detect large earthquakes and polar motion. Measurements with accuracy 10 ppb detect solid tides and plate tectonics on scales of decades. Measurements with accuracy of 1 ppb reveal the presence of the liquid core, crustal deformation caused by air and ocean mass distribution, and they allow to constrain parameters of the visco-elastic response of the mantle and physical properties of the core.

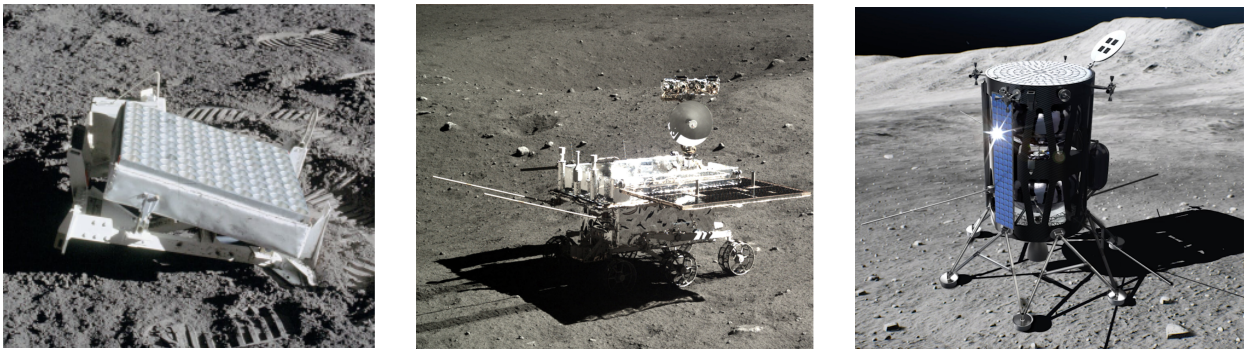

Figure 1: Instruments for selenodesy. *Left:* retroreflector installed by Apollo–11 mission operating since 1969. *Center:* radio beacon at Chang'E3 operating in 2015–2016. *Right:* radio beacon at LN–1 to be launched in 2022.

Geodetic observations on the Moon's surface have a similar potential to reveal dynamics of the Moon's crust. The absence of air and water on the Moon facilitates interpretation of crust

displacements and irregularities in the Moon's rotation. The era of selenodesy started in 1969 with a placement of the retroreflector on the Moon during NASA Apollo-11 mission (Bender et al., 1973; Dickey et al., 1994). At the moment, there are 5 retroreflectors on the Moon that form the fundamental selenodesy network. These retroreflectors are observed from the Earth's using the LLR technique (Currie et al., 2011; Murphy et al., 2012; Murphy, 2013) that determines travel time between a ground station and a retroreflector with a sub-centimeter level of accuracy.

These observations were used for improvement of the Lunar orbit (Folkner et al., 1994; Chapront et al., 2002; Williams et al., 2014; Williams and Boggs, 2016), for estimation of the Lunar rotation parameters called physical librations (Pavlov et al., 2016; Dumberry and Wieczorek, 2016), for determination of the Lunar crust displacements caused by tides (Williams and Boggs, 2015; Pavlov, 2020), Lunar core and its parameters (Meyer and Wisdom, 2011), and for testing fundamental physics theories (Turyshev et al., 2012; Williams et al., 2012; Hofmann and Müller, 2018). Analysis of lunar solid tides that reach $\pm$ 9 cm provides information on dissipation in the Moon's mantle at time scales that have not been probed by laboratory experiments and are only starting to be explored for the Earth (Matsumoto et al., 2015; Matsuyama et al., 2016; Harada et al., 2016). LLR first demonstrated that the Moon has a fluid core by detecting the energy dissipated by the flow of the fluid along the core mantle boundary from analysis of irregularities in the Moon rotation.

However, LLR has its own weakness. Observing from the ground an array of five retroreflectors on one side of the Moon that is always turned to the Earth makes problematic separations of variables that describe the Moon's orbital motion, rotation, and tides. This results in large correlation between estimates, which make interpretation of results difficult and less certain. New retroreflectors that are planned to be installed during future missions would be able to mitigate this problem to some extent, but will not eliminate it. The root of the problem is that retroreflectors see the Earth always at an angle that varies within several degrees while the coverage in a range of $\pm 180^\circ$ is optimal for variable separation.

The only other technique that is sensitive to Moon's orbital motion, rotation, and deformation is VLBI (Thompson et al., 2017). A network of ground radiotelescopes synchronously observe a radio-beacon or a natural extragalactic source such as active galactic nuclei (AGN). The VLBI data acquisition system digitizes voltage of received emission, records it on disk, and puts time stamps from ultra-stable atomic clock. The records are shipped to the analysis center and processed. The first stage of the data analysis computes the time series of cross- and auto-correlation functions. Processing these series determines delay of the wavefront arrival to station #2 with respect to station #1 with accuracy better than 1 cm (See Figure 2). VLBI observations are equivalent to differential one-way ranging between the radio beacon B and ground stations G_1 and G_2 that receive a signal emitted by B. The power of the VLBI technique for application to planetary sciences comes from its ability to process emission from both artificial beacons and natural radio sources, such as AGNs. Analysis of such observations allows us us to determine the angular displacement of the radio beacon with respect to an AGN direction. Since AGNs are located at gigaparsec distances (1 gigaparsec $\approx 3 \cdot 10^{22}$ meter), a coordinate system based on AGNs is inertial. Therefore, differential VLBI observations anchor the instantaneous lander position to the inertial space. Selecting an AGN at a small angular distance from the Moon allows to mitigate errors in path delay models in the ionosphere and the neutral atmosphere approximately by a factor of the angular distance between an AGN and the beacon expressed in radians.

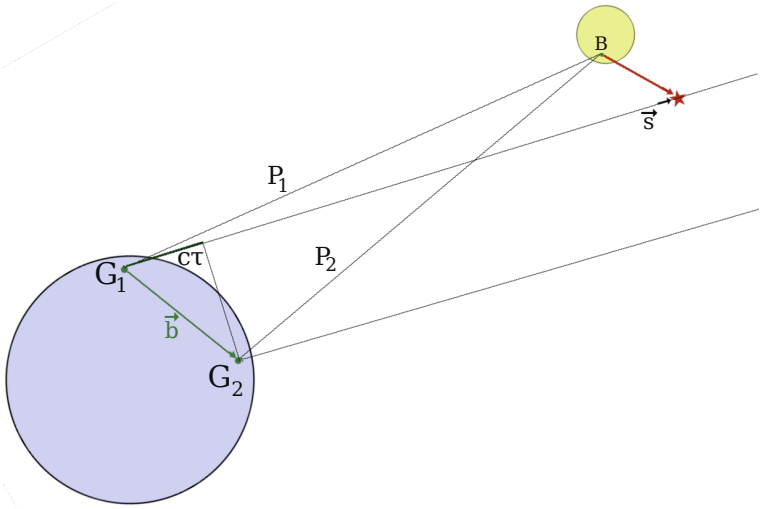

Figure 2: Geometry of VLBI observations. VLBI evaluates path delay $c\tau = |P_1| - |P_2|$ from the satellite and $c\tau = \vec{b} \cdot \vec{s}$ from a background extragalactic radio source. A projection of the unit vector of the source position to the celestial sphere is denoted with $\vec{s}$. Baseline vector $\vec{b}$ connects two ground stations G_1 and G_2. Differential observations of both lander B and the extragalactic source S allow us to determine precisely vector between B and S.

3 Motivation and problem statement

Although the potential of VLBI observations for planetary science was realized long time ago, progress was sluggish due to difficulties with data analysis. VLBI technique is commonly used for geodesy, for imaging of continuum spectrum sources such as AGNs, and for differential astrometry between two continuum spectrum source or between a continuum source and a narrow-band source, such as a stellar maser. When data from a continuum spectrum source is processed, the spectrum of cross-correlation is determined over the entire range of recorded bandwidth. Processing these data allows to evaluate precisely group delay since the error of group delay determination is reciprocal to the spanned bandwidth. Processing of a narrow-band emission from natural sources follows a different route, but it is based in the assumption that the frequency of the sources after accounting for the Doppler shift due to Earth's rotation and the orbital motion is constant. Processing of observations of Lunar landers cannot be reduced to processing of natural narrow-band sources because its frequency is changed due to both instability of the beacon signal and the contribution of the Doppler frequency shift. The frequency shift depends on beacon a priori positions that are usually not known with the accuracy that would prevent signal decorrelation.

We propose to develop the methodology for processing of differential VLBI observations of Lunar landers and AGNs. Phase referencing VLBI was successfully used for slow-moving interplanetary spacecrafts (Fomalont et al., 2010; Duev et al., 2012; Park et al., 2015; Jones et al., 2020), however its use for observations of a Lunar lander that moves quickly over the sky poses an additional challenge and it was not explored before. Based on the methodology outlined below, we will develop a tool that processes VLBI observations and produce a) time series of differential phases between a lander and an AGN, as well as their rate of change and b) time series of angular position offsets of the lander with respect to background AGNs.

The availability of such a tool will allow the planetary science community to process existing

VLBI observations of radio-beacons on the Moon and plan future observations of both dedicated beacons installed for navigation purposes and the signals of opportunity, such as telemetry of spacecrafts operating on the Moon surface. VLBI differential phase referencing data have a significant impact in the field of Lunar sciences for the following reasons. First, since VLBI data are independent of LLR, when analyzed separately, analysis of discrepancies can be used for LLR validation. Second, LLR and differential VLBI observables are sensitive to orthogonal projections of instantaneous lander positions and therefore, when analyzed together, synergism will be achieved, because combined use of orthogonal observables improves variable separation and improves robustness of results. Third, VLBI allows to get more dense time series, 200–2000 phase delays and rates points for an observing session within a given day, independent on weather, compare with 10–30 normal points per clear sky night from LLR observations.

The major motivation of our work is to lift barriers that impede proliferation of VLBI observations of spacecrafts on the Moon.

4 Methodology

VLBI observations of artificial signals from lunar landers can be done in three modes: a) phase tracking (Kikuchi et al., 2004; Sun et al., 2018), b) geodetic mode using group delays (ΔDOR) (Kikuchi et al., 2004; James et al., 2009), and c) phase referencing mode (Jones et al., 2020). Antennas continuously observe the lander in the phase tracking mode, and phase as a function of time is derived from correlation. Informational contents of such measurements is similar to integrated differential Doppler. Such measurements have a questionable value (See f.e., He et al., 2017, for more details).

Phase-referencing is the main technique in radio astronomy that is de facto a default mode. A scheme of phase-referencing observations is shown in Figure 3. In the simplest case the observing session consists of observing at the beginning and at the end strong amplitude calibrators that are called fringe finders. Observations are made in a sequence C-T-C-T- ... . All antennas of the array dwell on a phase calibrator (C) then slew to target (T), then back, etc. The period of time antennas collect the data is called a scan. Typical scan duration: 15–150 s. The sequence C-T-C-T- is periodically broken and antennas observe for some time atmospheric calibrators. These are call "geodetic blocks". In more sophisticated schemes, more than one phase calibrator is used. The use of more than one calibrator allows to mitigate substantially the impact of residual propagation delay. Such observations are made in a scheme C1-T-C1-C2-T-C2-T-C1- ... or C1-T-C1-C2-T-C2-C3-T-C3-C1- ... . Calibrators are selected within 1–3° of a target (Martí-Vidal et al., 2010). Geodetic blocks last 7–30 minutes and are repeated every 1–5 hours.

Since the Moon is moving with respect to the inertial space with a rate of approximately 30′ per hour, the angular distance of a beacon with respect to calibrators is evolving. The network of observing stations is changed when the Moon is setting at some station and rising at others. Therefore, observations are organized with blocks of 30–50 minutes long. The next block may have different stations and/or different calibrators.

The primary goal of this project is to develop an algorithm that will process phase referencing observations of a lunar lander and evaluate a position offset of the beacon on the lander with respect to natural extragalactic radio sources used as calibrators. The data analysis procedure has a number of steps and each step is refining results obtained at the previous step.

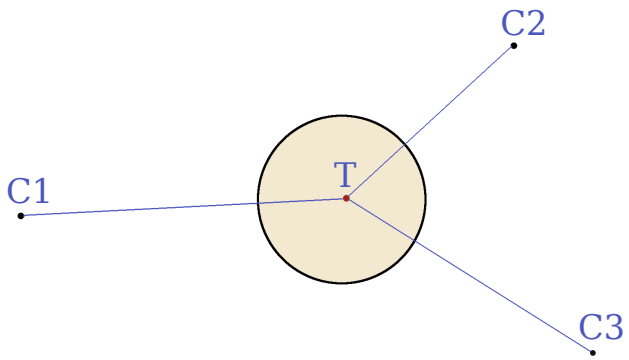

Figure 3: Scheme of nodding observations of spacecraft (T) that transmits narrow-band emission and background AGNs (C1, C2, and C3) that emit in the continuum.

4.1 Correlation

Data with records of digitized voltage from receivers are processed with the so-called software correlator, program DiFX (Deller et al., 2007, 2011) supported by the radio astronomy community. This software is adequate for processing data from calibrators. The only change that is needed is to perform precise computation of path delay from the lander. An extragalactic source is located in the far zone, and path delay is computed assuming the wavefront is parallel Kopeikin and Schäfer (1999). That approach is not applicable for observing object in the near zone. We will develop program sf difx_nz for computation of path delay for the beacon with selenocentric a priori position $\vec{B}$ observed from ground stations G_1 and G_2 at the moment t_1 of the arrival of the wavefront to G_1. Here is the pseudo code:

- compute Moon position $\vec{M}$ and velocity $\dot{\vec{M}}$ at t_1 in the celestial coordinate system (CCS)
- compute Moon rotation and Earth rotation matrices $\widehat{\mathcal{R}}_{\oplus}$ and $\widehat{\mathcal{R}}_{m}$ at t_1
- compute position of ground stations and the lander in CSS at t_1
- compute travel time $\tau_1 = |BG_1|(t_1)$ and $\tau_2 = |BG_2|(t_1)$
- compute position of the lander at $t_1 - \tau_1$ and position of G_2 at $t_1 - \tau_1 + \tau_2$
- repeat previous three steps till convergence is reached

Implementation will be based on software package VTD that we previously developed for processing VLBI data of extragalactic sources. We have developed an analytical expression for this procedure as well (Jaron and Nothnagel, 2018).

The correlation is performed with some initial coarse path delay model. We will develop software for preprocessing raw output of the the time series of the cross-correlation spectrum also known as visibilities. This will include computation of corrections for the difference $\Delta\tau$ between a precise path delay computed as described above and the one used as a priori during correlation by applying a phase rotation $e^{i2\pi f \Delta\tau(t)}$, where f is the cyclic frequency, splitting the data into observations to the lander and calibrator sources, performing initial quality control, and writing updated dataset for further analysis.

The principal difficulty in processing of lander observations is that the lander is moving with respect to the inertial system because of Moon's orbital motion and rotation. Applying the a priori Moon's ephemeride and a priori lander positions reduces the residual motion but does not stop

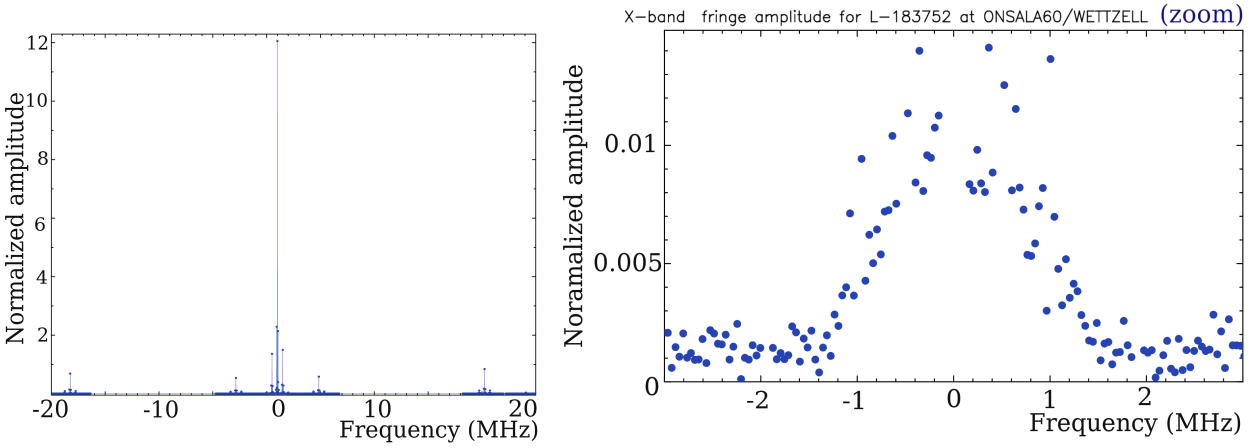

Figure 4: *Left* Amplitude spectrum of the the signal from Chang'E3 lander within 20 MHz bandwidth centered at 8.47 GHz. *Right:* zoom of the spectrum near the signal carrier. This plots does not show a number of narrow-band spectral constituents that are beyond the plotting area.

it. In order to reach the target accuracy, visibility data should be accumulated and coherently averaged. Coherent averaging requires phase be stable within the averaging interval. That requires knowledge of improved lander position. This is a non-linear problem, specific for the planetary VLBI observations, and is solved with iterations. The solution we propose is outlined below.

4.2 Processing group delays

Figure 4 shows spectrum of Chang'E3 lander which is typical. The signal consists of the narrow-band carrier, a number of additional narrow-band tones, and the broad-band constituents with a spectrum shape close to the Gaussian function. The width of emitted narrow-band tones range within 0.01–100 Hz depending on the emitter hardware, and the tones are spread over 10–100 MHz. The broad-band signal has the width of about 1 MHz and is associated with a telemetry channel. These constituents are processed separately.

First, observations of calibrator sources are processed in a usual way of analysis of continuum spectrum objects. During that stage phase delay τ_p, phase delay rate $\dot{\tau}_p$, and group delay τ_g are adjusted using all the cross-correlation time series of a given scan in such a way that the coherent sum of weighted complex cross-correlation samples c_{kj}

$$C(\tau_p,\tau_g,\dot{\tau}_p) = \sum_k \sum_j c_{kj}\, w_{kj}\, e^{i(\omega_0\tau_p + \omega_0\dot{\tau}_p(t_k-t_0) + (\omega_j-\omega_0)\tau_g)} \qquad (1)$$

reaches the maximum amplitude. Index k runs over time, and index j runs over frequencies. ω_0 and t_0 denote reference circular frequency within the band and the reference time within a scan, ω_j is the subband frequency, and w_{kj} are weights. Then using estimates of group delays and phase delay rates, the visibilities are averaged over time and frequency with the specified averaging intervals, and the averaged visibilities are used for reconstruction of radio-images of phase calibrators in a form of two-dimensional brightness distributions $B(x,y)$.

Second, broad-band group delay from lander observations is computed using a portion of the spectrum with the lander broad-band signal by maximizing $C(\tau_p,\tau_g,\dot{\tau}_p)$ in Eq. 1 using the

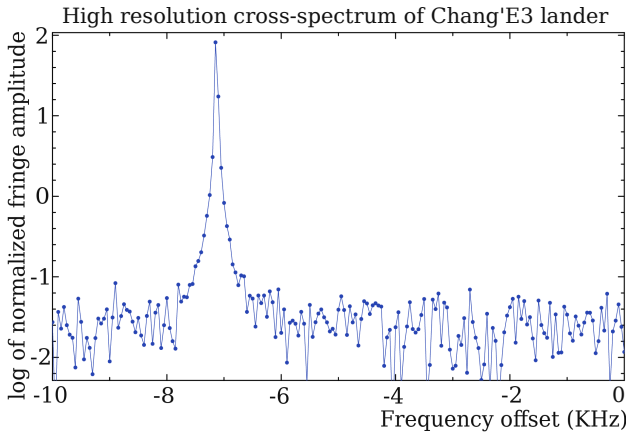

Figure 5: Cross-spectrum of the Chang'E3 carrier with resolution 50 Hz centered at 8.47 GHz.

common fringe fitting procedure (Petrov et al., 2011a). Since the bandwidth of the lander board-band spectrum is usually narrower than the recorded bandwidth, the spectrum is multiplied by a mask that consists of 0 and 1 to limit the dataset with the data that contains the signal from the lander. In a case if the lander spectrum is not a priori known, the procedure for determination of the bandwidth based in analysis of autocorrelation runs. This procedure computes the noise level in the frequency band where no signal is expected and finds the portion of the auto-spectrum that deviates by N times of the root mean square of the noise.

Broad-band group delays from observations of calibrators and the lander are processed in the same fashion as in geodetic VLBI analysis. Clock function, atmospheric path delay in zenith direction, and correction to a priori selenocentric lander positions are adjusted in a least square using group delays. Depending on the design of observations and the spectrum of the emitted signal, position accuracy of a Lunar lander determined that way ranges from 10 to 1000 meters. The adjusted parameters form the basis for further refinement.

These blocks of the computational procedures are already developed and they are used for processing routine geodetic and astronomical observations. We plan the following work: a) to upgrade existing software for path delay computation to support a lander on a different planet; b) to develop software that calls computational blocks within a pipeline that combines observations of calibrators and the lander; c) to develop a database that would hold results of these computations and intermediate results; d) to develop quality control procedures that would determine outliers in lander observations and flag bad data.

4.3 Processing phase delays and delay rates

A lander has a narrow band signal from the carrier. Determination of the phase of this signal is the goal of this stage of data analysis. Phase delays are a factor of 10–100 more precise than group delays, but have ambiguities with spacings c/f that are 3.4 cm for Chang'E3 observations.

Frequency of the carrier signal is changing in time. It has a regular constituent due to Doppler shift and a jitter due to the instability of the on-board frequency standard. The a priori model used for correlation subtracts the known part of the Doppler shift, but it retains the residual Doppler shift due to an uncertainty in lander position. Because of these factors, the spectrum of the carrier broadens (See Figure 5).

We filter out a part of the spectrum that contains the signal from the carrier within $[\omega_o -$

$\omega_b, \omega_o + \omega_b]$ frequency range, where ω_o is the frequency of the maximum. If the model were perfect and the frequency oscillator had no jitter, the interferometer response, i.e. the inverse Fourier transform of the cross-spectrum, would be $\cos(\omega_0 \tau_p)$. We represent the inverse Fourier transform of the cross-spectrum $\mathcal{F}^{-1}(C(t,\omega))$ as

$$\mathcal{F}^{-1}(C(t,\omega)) = A\cos\left(\omega_0 \cdot \left(1 + \sum b_i B_i^k(t)\right) \cdot \left(\tau_p + (t-t_0)\dot{\tau}_{pj} + \frac{1}{2}(t-t_0)^2\ddot{\tau}_p\right)\right), \qquad (2)$$

where $B_i^k(x)$ is the basic spline of the kth degree. We will fit b_i, τ_p, $\dot{\tau}_p$, $\ddot{\tau}_p$ using the inverse Fourier transform of time series of the cross-spectra of a given scan within the frequency range $[\omega_o - \omega_b, \omega_o + \omega_b]$. We will perform non-linear least squares fit using initial values of τ_p and $\dot{\tau}_p$ determined at the previous step of data analysis. We will evaluate initial values of b_i using visibility amplitudes.

We will use unambiguous $\dot{\tau}_p$ and $\ddot{\tau}_p$ collected from all the scans to further refine lander position, and then we will repeat steps of determination of group delay followed by determination of phase delays with updated a priori model of lander positions.

We will develop new software for these steps. That will include search of the frequency range of the carrier $[\omega_o - \omega_b, \omega_o + \omega_b]$, parameter estimation, outlier detection, quality control, and bookkeeping.

4.4 Determination of multi-tone group delay

In a case if the lander signal has other narrow-band tones than the carrier, the multi-tone group delay is determined. For instance, Chang'E3 has 18 side tone with frequencies in range of ± 19.75 MHz with respect to the nominal carrier frequency 8470 MHz that can be used for data analysis.

We represent the inverse Fourier transform of time series of the cross-spectrum of the side-band tone j at the nominal circular frequency $\omega_0 + \Delta\omega_j$ in the same form as in Eq. 2, and process then in a similar way the main carrier, but we do not estimate coefficients b_i, $\dot{\tau}_p$ and $\ddot{\tau}_p$ keeping them fixed to the values determined from processing the signal carrier. We adjust only correction to frequencies $\Delta\omega_j$ and phase delays τ_{pj} for each side-band tone using least squares.

The array of phase delays τ_{pj} and their uncertainties determined from the scatter of processed visibilities, as well as the phase delay of the signal carrier are used for evaluation of the multi-tone group delay τ_{mg} and multi-tone phase delay τ_{mp} using weighted least squares with weights set to be reciprocal to phase delay uncertainties:

$$\omega_j \tau_{pj} = \omega_0 \tau_{mp} + (\omega_j - \omega_0)\tau_{mg}. \qquad (3)$$

Since precision of group delay is reciprocal to the spanned bandwidth, precision of multi-band group delay is greater than precision of broad- band group delay. Spanned bandwidth of Chang'E3 broadband signal is ~ 2 MHz and spanned bandwidth of side-band tones is 39.5 MHz.

We will develop new software to implement these steps of the data analysis pipeline. That will include search for suitable side-band tones, computation of τ_{pj}, evaluation of their uncertainties, outlier detection, quality control, bookkeeping and computation of the multi-band group delay.

4.5 Forming phase delay differences

After the best estimates of phase and group delays from the lander are computed, differential phase and group delays between observations of calibrators and the lander are calculated. First the contributions of source structure to phase and group delays of calibrators τ_{str} are computed for given observations using the 2D Fourier transform of their brightness distribution (Charlot, 1990). These contributions account for deviation of source brightness distribution from δ-function. They are subtracted from delays computed during fringe fitting. Then time series of phase delays, phase delay rates and group delays of a calibrator are expanded into basis spline functions with applying smoothing constraints, and group and phase delays of calibrators are interpolated to middle epochs of scans of lander observations (See Figure 6).

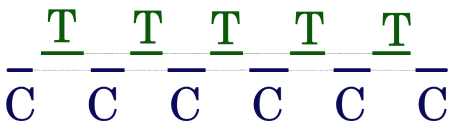

Figure 6: Illustration of phase referencing observations. The array observe target (T) then slews to a calibrator (C). The cycle is repeated. Fringe phases of the target and the calibrator are shown with a thick line. They are interpolated (thin lines) and phase differences are computed for a number of epochs.

The time series of differential phase and group delays are produced by differencing data from the calibrator and the lander referred to the common epoch and common frequency. These differential phase and group delays form the basis for further analysis.

We will develop new software for interpolation of phase and group delays of calibrators sources and computation of differential phase and group delays. We will incorporate existing imaging software into the data analysis pipeline.

4.6 Differential imaging

Ambiguities in differential phase delay have to be resolved before their use in the geodetic analysis. This is a critical part of the analysis. The feasibility of resolving phase delay ambiguity depends on the signal spectrum, signal strength, and experiment design. A general approach is to use group delay as a starting point with imposing constraint. Differential group delay of a signal from the broad-spectrum constituent of the lander signal (See right plot in Figure 4) of the lander is unambiguous. The multi-tone group delays of the lander have ambiguities that are reciprocal to the minimum frequency difference between tones. Since mutli-tone group delay ambiguity spacings are large (15.6 μs or 4.7 km for Chang'E3), broad-band group delays are precise enough to resolve these ambiguities.

If accuracy of the broad-band or multi-tone delays is better than 1/6 of the ambiguity spacing that is reciprocal to the carrier frequency (118 ps or 4 cm for Chang'E3), then ambiguities are resolved easily. In other cases additional information should be used to provide constraints.

At all previous steps cross-correlation from observations at different baselines was processed separately. The ambiguity resolution process commences with a transformation of baseline-based differential phases to station-based phases and then back to baseline-based quantities. The closure condition $\tau_{12} - \tau_{13} + \tau_{23} = 0$ referred to the same time epoch is held for a path delay related to

the common epoch at baselines between any three stations. This process eliminates integer ambiguities that would break the closure conditions. Then, the visibility data are gridded, amplitude is replaced with a constant 1 Jy, and a hybrid imaging process is executed using only the phase self-calibration loop. If the image quality is good, then its maximum provides the lander angular position offset at the reference epoch with respect to the latest a priori model used. The lander position is fitted to that angular offset, the updated model is applied, updated phase delays are computed, and the phase delay ambiguity is resolved with respect to the predicted phase. These phase delays are used for the final parameter adjustment and assessment of the position errors.

The true image of the lander is expected to be a δ-function. Phase noise in the image will cause a deviation of the image from the δ-function. The sparseness of observations will cause peaks and negative flux densities. Inaccuracy in a priori lander positions will cause residual motion of the lander with respect to the calibrator, which will result in image smearing. Figure 7 shows dirty image (i.e. before phase and amplitude self-calibration) of AGN J1458+1427 that was observed in one scan at a 5-station VLBA sub-network using 60 second integration time as an illustration of how a raw lander radio-image recovered from VLBI data may look.

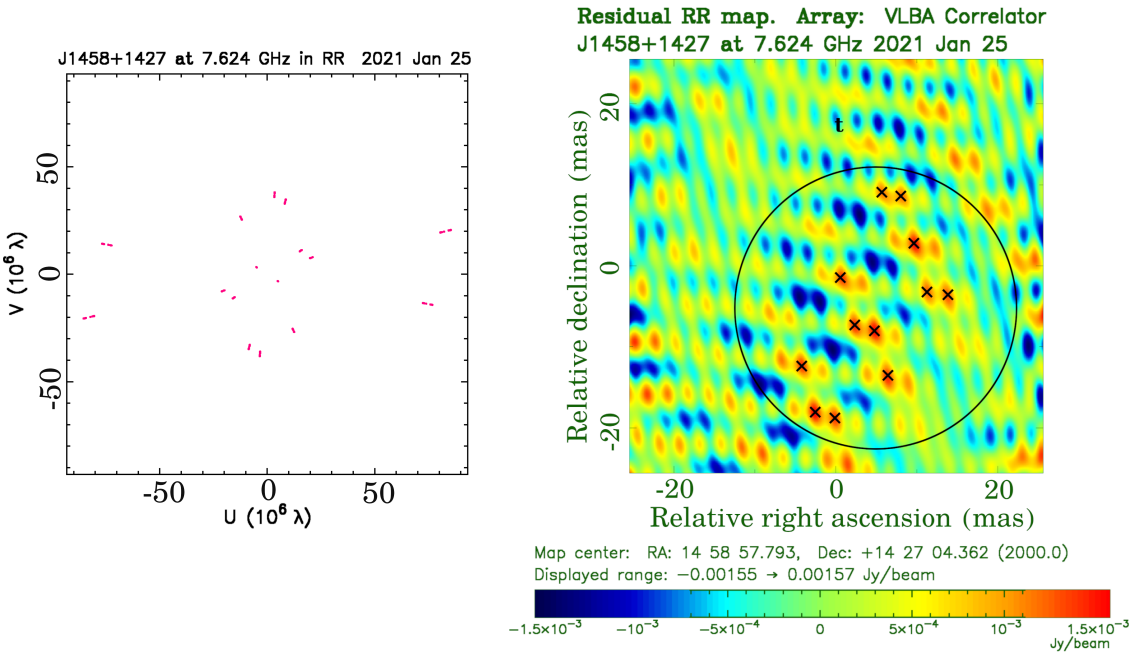

Figure 7: Example of a dirty image. *Right:* Dirty image of J1458-1427 in a snap-short observation at a 5-station VLBA sub-network before phase self-calibration. × sign shows maxima at the image. *Left:* *uv*-coverage of these observations.

This image shows a number of maxima. However, the previous adjustment of the lander position limited the number of maxima to consider. A black circle in Figure 7 shows errors from inferred from positions adjustments for illustrative purposes. Maxima above some level with respect to the main maximum are shown with sign ×. A coordinate of each point on an image is tied to the position of the calibrator that is taken from the catalogue of absolute AGN positions that was determined in numerous programs of absolute astrometry for last 25 years (Beasley et al., 2002; Fomalont et al., 2003; Petrov et al., 2005, 2006; Kovalev et al., 2007; Petrov et al., 2008;

Condon et al., 2017; Petrov and Taylor, 2011; Schinzel et al., 2015, 2017; Fey and Charlot, 1997; Petrov et al., 2011a,b; Petrov, 2011, 2012, 2013; Gordon et al., 2016; Shu et al., 2017; Petrov et al., 2019; Popkov et al., 2020; Petrov, 2021). The algorithm checks all maxima and for each maximum executes the following procedure. First, it determines right ascension and declination of the maxima in the inertial coordinate system from the image. Second, it adjusts lander positions in the selenocentric coordinate system. Third, it computes path delay using adjusted positions for all used observations. Fourth, it forms residuals between computed path delays and observed differential phase and group delays between computed path delay rate and observed path delay rate. Fifth, the algorithm finds a set of N admissible integer ambiguities for each observable at a given baseline and a given scan. Parameter N can be set to a range of 2 to 10, depending on data quality. Sixth, the algorithms computes statistics of residuals. In a case of correctly resolved phase delay ambiguities, the differential phase delay residuals have zero mean and the standard deviation that is consistent with the noise in data and residual atmospheric fluctuations. In a case of incorrectly resolved ambiguities, differential phase delay residuals are biased and have an excessive scatter. The algorithm evaluates the probability of false selection of the integer ambiguity based on statistics of the residuals. All maxima at the image are examined and that maximum that provides the minimum of the probability of false phase delay ambiguity among all admissible maxima is selected. As a results of this process, ambiguity-free estimates of phase delay and improved estimates of lander positions are computed. Improved positions of the lander are used for re-computation of differential phase delays and re-imaging the lander. Then the procedure is repeat. The iterations are stopped when convergence is reached.

We expect image quality of the lander over 30 or 50 minute integration time will be better than at Figure 7, but we our algorithm is expected to converge to a solution that even in a case of a poor image. Imaging the lander dramatically reduces the number of admissible combinations of integer ambiguities.

We will develop software for implementation of the above algorithm. We will develop software that examines probability of false ambiguity resolution, computes uncertainties of phase and group delays, positions of the lander, and examine convergence.

4.7 Analysis of differential phase delays

The time series of differential phase delays $\Delta\tau_p$, phase delay rates $\Delta\dot{\tau}_p$, and phase delay accelerations $\Delta\ddot{\tau}_p$ are used for a final estimation of lander positions using least squares. Then adjustments of lander positions, phase delay ambiguities, as well as parameters of the signal carrier frequency jitter b_i, are used as a priori for the last round of data analysis of the original visibility data with applied outliers flagging. Inaccuracy in the a priori lander position resulted in a residual motion of the lander. That residual motion is eliminated in the final round of data analysis.

Analysis of residual visibilities allows to compute errors in phase delays and phase delays rates. The outcome of this analysis are a) improved lander position and estimates of its uncertainty; b) time series of ambiguity free differential phase delays, group delays, phase delay rates and phase delay acceleration, as well as their uncertainties; c) angular offsets of the lander with respect observed calibrator sources.

We will develop software for computation of the final position of the lander and its position offset with respect to calibrator sources. We will develop software that will generate database files in VGOSDB format adopted by the International VLBI Service for Geodesy

and Astrometry and put there a) time estimates of phase delay, phase delay date, phase acceleration, group delays; b) time series of lander angular position offsets with respect to calibrator sources; and c) auxiliary information about VLBI observations that is present in VGOSDB databases.

5 Proposed work

We aim to develop a semi-automated tool PlaVDA that would ingest the correlator output of VLBI observations of a lander and extragalactic sources that can be considered as a Level 1 data product and compute observables that are suitable for scientific analysis in depth: time series of differential phase delays, phase delay rates, group delay as well as a by-product updated positions of the lander. These observable can be considered as a Level 2 data product and they become an input for a combined analysis of VLBI and LLR observations for adjustments of parameters of Lunar tides, improvement of the Moon orbit and other quantities using existing tools such as Geodyn and GINS. Scientific analysis of Level 2 data is beyond the scope of the proposed work.

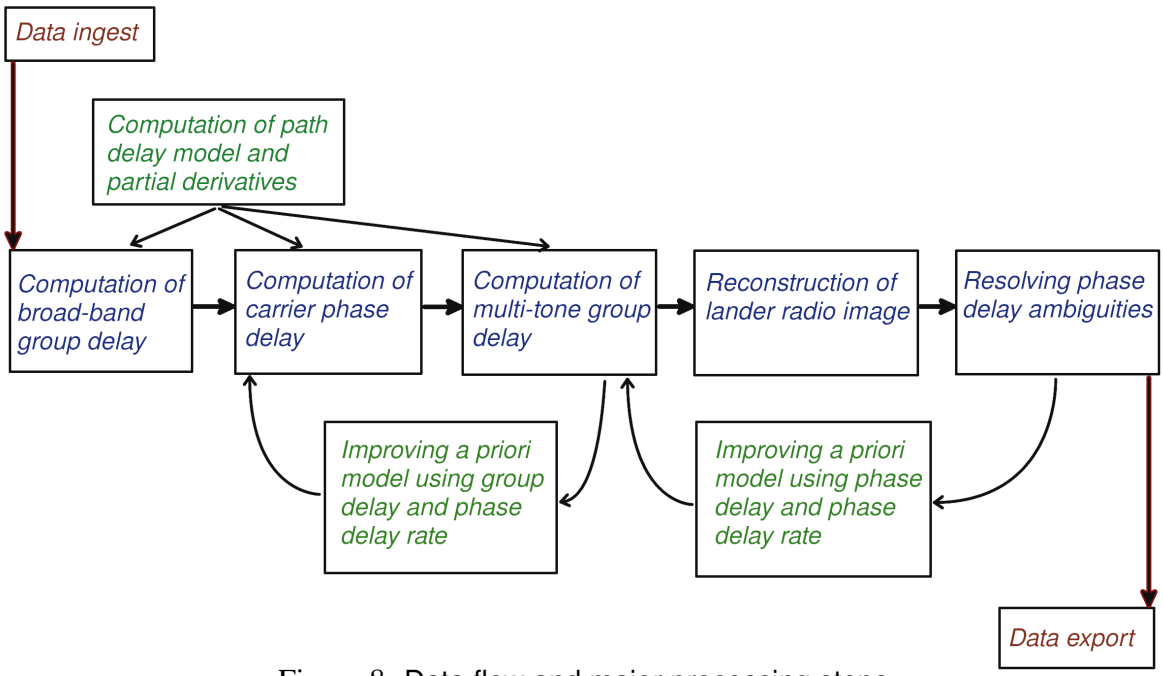

Figure 8: Data flow and major processing steps

We will use existing open source tools of VLBI data analysis, specifically, VLBI Time Delay (VTD) library for computation of path delay for extragalactic sources, PIMA — a general purpose fringe fitting software, and DifMAP — a general purpose differential VLBI image software and adapt them for solving the problem of producing ambiguity-free differential phase and group delays. Specifically, we will develop algorithms and implementation them in software for

- computation of path delay of an object on the Moon or other body in the Solar System;
- estimation of position of an object on the Moon or other body in the Solar System using path delay;
- evaluation of phase delay from a carrier and side-band tones of an object with residual motion such as a Lunar lander;

- resolving phase delay ambiguity and evaluation of the probability of using a preliminary image of the lander corrupted by artifacts due to its residual motion;
- quality control of each step that includes detection of outliers, their flagging, estimation of probability of false detection and false ambiguity resolution.

We will develop the pipeline software that will combine existing software programs and those that we will develop for processing Lunar lander data in one package PlaVDA. PlaVDA will execute all the steps described above. It will take the initial cross-correlation data and generate the output database file in VGOSDB format with results of analysis. PlaVDA will accept a plain ascii control file in a format `keyword: value` that describes all steps of the data analysis. Due to scarcity of available VLBI data suitable for validation, efforts for developing a fully automatic tool are not justified. We adopt a guided semi-automatic data analysis approach. That means that PlaVDA control file in part will be created manually and in part by other programs. A user will have an ability to insert break points in the pipeline, examine results, if necessary, amend the control file and rerun it. By the end of this guided run, the full control file will be created. That file will allow a user to run PlaVDA in a totally automatic fashion. That approach will allow to reproduce results.

5.1 Validation

We will be using two experiments from the OCEL campaign (Observing the Chang'E3 Lander with VLBI) run on 2015–2016 for validation of PlaVDA package. These data are publicly available at CDDIS [1]. Huang et al. (2014); Han et al. (2019a,b); Klopotek et al. (2019) performed analysis of group delays and reached position accuracy 3–10 meters. These results demonstrate that the data are high quality. The experiment included block of phase referencing observations. The authors of the cited papers did not make an attempt to work with phase delays and did not provide publicly accessible tools. We will go beyond what Han et al. (2019a); Klopotek et al. (2019) have achieved, process phase delays, and make the tools and results of our analysis publicly available.

We expect accuracy of phase delay analysis will be higher than 3–10 meters. Statistics of lander positions collected from analysis of 10 observing sessions will allow us to evaluate the scatter of estimates. Statistics of this scatter will allow us to draw an inference about validity of our approach and whether accuracy of phase delays meet expectations.

5.2 Data management

The input Level 1A data that we will be using for validation are archived at the Crustal Dynamics Data Information System (CDDIS) together with VLBI data for space geodesy. The CDDIS provides tools for data ingest, search, and performs backup. The CDDIS mission is to keep the data for the scientific community indefinitely. It provides access to format descriptions. Future VLBI Lunar lander observations will be archived as CDDIS.

The output of processing Level 1A data in a form suitable for planetary data analysis, Level 2 data, will be archived at CDDIS using established VGOSDB format adopted by the geodetic community for archiving all Level 2 VLBI geodetic data. Therefore, users that are interested in VLBI data will expect to find lander VLBI data for selenodesy there.

[1] See as an example https://cddis.nasa.gov/archive/vlbi/ivsdata/swin/2015/20151201_rd1510_v001_swin.tar.bz2

Source code developed in the framework of this project will be deposited to https://github.com/nasa under Apache License 2.0.

5.3 Prior work

The team has an extensive experience in processing VLBI data for geodetic and astronomical observations. We have developed software VTD, PIMA, pSolve for data analysis of extragalactic sources and processed over 6000 geodetic VLBI experiments and 1000 astronomy observations. We have extensive experience in imaging active galactic nuclei from VLBI observations. We ran a preliminary analysis of VLBI experiments from the OCEL campaign an familiarized ourselves with these data.

5.4 Risk mitigation

Resolving phase delay ambiguities always brings a risk of a failure. Feasibility of phase delay resolution depends on a level of unaccounted errors: if there are systematic errors that are a substantial fraction of the ambiguity spacing, for instance to due instrumental errors in VLBI hardware, then ambiguity resolution is not feasible. Our approach with estimation of the probability of false ambiguity resolution is design to detect such a situation and provide a measure of the phase delay scatter. In a case if the phase delay scatter is low, and therefore, phase delay ambiguity resolution is feasible, there is a risk that the initial lander position based on group delay may be biased. Our approach of generation of a lander image and running a the ambiguity resolution procedure using maxima on the image as an initial value will mitigate the risk.

5.5 Future observations

Our validation plan is based on publicly available observations and does not depend on other observations. At the same time, the National Radio Astronomical Observatory has awarded to our teem observing time with the Very Long Baseline Array for observations of Lunar Node–1 Payload on the Intuitive Machines NOVA-C Lander (LN–1) in 2022. This opportunity to collect new data and analyze them provides us an additional motivation to develop PlaVDA tool. LN–1 does not bring an instrument payload manufactured for VLBI — we will be observing the telemetry signal. With an expectations of many space vehicles be landing on the Moon within this decade, an opportunity emerges to perform selenodesy observations almost for free, provided planetary scientists have a tool for processing these data.

6 Deliverables and Outcomes

In a course of the project we will

- develop software tool PlaVDA for processing Level 1A VLBI observations of a Lunar lander. The tool will compute group delays, phase delay, and phase delay rates at a range of epochs and generate Level 2 product in VGOSDB format. We will make the source code of that tool publicly available at https://github.com/nasa.
- process two VLBI experiment of observing Chang'E3 lander and submit Level 2 data product at CDDIS.
- validate Level 2 data product using NASA Geodyn software.
- prepare NASA Technical Memorandum with a detailed algorithm description.
- submit a paper to a refereed journal that describe PlaVDA and results of Level 2 validation.

7 Management plan and milestones

The chart below shows the schedule for implementing the tasks. The schedule is arranged to give an approximately uniform deployment of effort for the team.

Table 1: Schedule chart

Activity name	PY1	PY1	PY3
Development of algorithms for processing group delays	•		
Development of algorithms for processing phase delays	•	•	
Processing existing VLBI data and the tool validation		•	•
Writing papers and reports			•

The Principal Investigator, Leonid Petrov, geophysicist in Geodesy & Geophysics Laboratory (Code 61A) at NASA GSFC will manage the project. He will coordinate the efforts of the team. Leonid Petrov will develop algorithms, design the software tool, and work on implementing the algorithms into software together with the software developer. He will design the test suite.

The co-I Vishnu Viswanathan, will ...

The co-I Frank Lemoine, at NASA GSFC Code 61A, will perform validation of the PlaVDA results of processing VLBI observations of Chang'E3 using Geodyn.

The software developer, TBD, will work with the PI on coding PlaVDA and testing the code.

The collaborator Erwan Mazarico, geophysicist of NASA GSFC, Code 698 will ...

The collaborator Frederic Jaron will ...

The collaborator Rüdiger Haas, the principal investigator of VLBI OCEL campaign, with consult the team about details of these observations.

All teams members will be contributing in writing a technical memorandum and the journal paper.

8 References

Beasley, A. J., D. Gordon, A. B. Peck, L. Petrov, D. S. MacMillan, E. B. Fomalont, and C. Ma (2002), "The VLBA Calibrator Survey-VCS1." *Astrophys. J. Suppl. Ser.*, 141, 13–21 doi: 10.1086/339806.

Bender, P. L., D. G. Currie, S. K. Poultney, C. O. Alley, R. H. Dicke, D. T. Wilkinson, D. H. Eckhardt, J. E. Faller, W. M. Kaula, J. D. Mulholland, H. H. Plotkin, E. C. Silverberg, and J. G. Williams (1973), "The lunar laser ranging experiment." *Science*, 182, 229–238 doi: 10.1126/science.182.4109.229.

Chapront, J., M. Chapront-Touzé, and G. Francou (2002), "A new determination of lunar orbital parameters, precession constant and tidal acceleration from LLR measurements." *Astronomy & Astrophysics*, 387, 700–709 doi: 10.1051/0004-6361:20020420.

Charlot, P. (1990), "Radio-source structure in astrometric and geodetic very long baseline interferometry." *Astron. J.*, 99, 1309–1326 doi: 10.1086/115419.

Condon, J. J., J. Darling, Y. Y. Kovalev, and L. Petrov (2017), "A Nearly Naked Supermassive Black Hole." *Astrophys. J.*, 834, 184 doi: 10.3847/1538-4357/834/2/184.

Currie, Douglas, Simone Dell'Agnello, and Giovanni Delle Monache (2011), "A lunar laser ranging retroreflector array for the 21st century." *Acta Astronautica*, 68, 667–680 doi: 10.1016/j.actaastro.2010.09.001.

Deller, A. T., W. F. Brisken, C. J. Phillips, J. Morgan, W. Alef, R. Cappallo, E. Middelberg, J. Romney, H. Rottmann, S. J. Tingay, and R. Wayth (2011), "DiFX-2: A More Flexible, Efficient, Robust, and Powerful Software Correlator." *Publ. Astron. Soc. Pacific*, 123, 275 doi: 10.1086/658907.

Deller, A. T., S. J. Tingay, M. Bailes, and C. West (2007), "DiFX: A Software Correlator for Very Long Baseline Interferometry Using Multiprocessor Computing Environments." *Publ. Astron. Soc. Pacific*, 119, 318–336 doi: 10.1086/513572.

Dickey, J. O., P. L. Bender, J. E. Faller, X X Newhall, R. L. Ricklefs, J. G. Ries, P. J. Shelus, C. Veillet, A. L. Whipple, J. R. Wiant, J. G. Williams, and C. F. Yoder (1994), "Lunar laser ranging: A continuing legacy of the apollo program." *Science*, 265, 482–490 doi: 10.1126/science.265.5171.482.

Duev, D. A., G. Molera Calvés, S. V. Pogrebenko, L. I. Gurvits, G. Cimó, and T. Bocanegra Bahamon (2012), "Spacecraft VLBI and doppler tracking: algorithms and implementation." *Astronomy & Astrophysics*, 541, A43 doi: 10.1051/0004-6361/201218885.

Dumberry, Mathieu and Mark A. Wieczorek (2016), "The forced precession of the moon's inner core." *Journal of Geophysical Research: Planets*, 121, 1264–1292 doi: 10.1002/2015je004986.

Fey, Alan L. and Patrick Charlot (1997), "VLBA Observations of Radio Reference Frame Sources. II. Astrometric Suitability Based on Observed Structure." *Astrophys. J. Suppl. Ser.*, 111, 95–142 doi: 10.1086/313017.

Folkner, W. M., P. Charlot, M. H. Finger, J. G. Williams, O. J. Sovers, Xx Newhall, and Jr. Standish, E. M. (1994), "Determination of the extragalactic-planetary frame tie from joint analysis of radio interferometric and lunar laser ranging measurements." *Astron. & Astrophys.*, 287, 279–289.

Fomalont, E., T. Martin-Mur, J. Border, C. Naudet, G. Lanyi, J. Romney, V. Dhawan, and B. Geldzahler (2010), "Spacecraft navigation using the VLBA." In *10th European VLBI Network Symposium and EVN Users Meeting: VLBI and the New Generation of Radio Arrays*, vol. 10, 66.

Fomalont, E. B., L. Petrov, D. S. MacMillan, D. Gordon, and C. Ma (2003), "The Second VLBA Calibrator Survey: VCS2." *Astron. J.*, 126, 2562–2566 doi: 10.1086/378712.

Gordon, D., C. Jacobs, A. Beasley, A. Peck, R. Gaume, P. Charlot, A. Fey, C. Ma, O. Titov, and D. Boboltz (2016), "Second Epoch VLBA Calibrator Survey Observations: VCS-II." *Astron. J.*, 151, 154 doi: 10.3847/0004-6256/151/6/154.

Han, Songtao, Axel Nothnagel, Zhongkai Zhang, Rüdiger Haas, and Qiang Zhang (2019a), "Fringe fitting and group delay determination for geodetic VLBI observations of DOR tones." *Advances in Space Research*, 63, 1754–1767 doi: 10.1016/j.asr.2018.11.018.

Han, SongTao, ZhongKai Zhang, Jing Sun, JianFeng Cao, Lue Chen, Weitao Lu, and WenXiao Li (2019b), "Lunar radiometric measurement based on observing china chang'e-3 lander with VLBI—first insight." *Advances in Astronomy*, 2019, 1–10 doi: 10.1155/2019/7018620.

Harada, Yuji, Sander Goossens, Koji Matsumoto, Jianguo Yan, Jinsong Ping, Hirotomo Noda, and Junichi Haruyama (2016), "The deep lunar interior with a low-viscosity zone: Revised constraints from recent geodetic parameters on the tidal response of the moon." *Icarus*, 276, 96–101 doi: 10.1016/j.icarus.2016.04.021.

He, Qing-bao, Qing-hui Liu, Sheng-qi Chang, and Xin Zheng (2017), "A New Try of Connecting Phase and Solving Phase Delay in VLBI." *Chin. Astron. and Astrophys.*, 41, 614–625 doi: 10.1016/j.chinastron.2017.11.011.

Hofmann, F and J Müller (2018), "Relativistic tests with lunar laser ranging." *Classical and Quantum Gravity*, 35, 035015 doi: 10.1088/1361-6382/aa8f7a.

Huang, Yong, Shengqi Chang, Peijia Li, Xiaogong Hu, Guangli Wang, Qinghui Liu, Weimin Zheng, and Min Fan (2014), "Orbit determination of chang'e-3 and positioning of the lander and the rover." *Chinese Science Bulletin*, 59, 3858–3867 doi: 10.1007/s11434-014-0542-9.

James, Nick, Ricard Abello, Marco Lanucara, Mattia Mercolino, and Roberto Maddè (2009), "Implementation of an ESA delta-DOR capability." *Acta Astronautica*, 64, 1041–1049 doi: 10.1016/j.actaastro.2009.01.005.

Jaron, Frédéric and Axel Nothnagel (2018), "Modeling the VLBI delay for earth satellites." *Journal of Geodesy*, 93, 953–961 doi: 10.1007/s00190-018-1217-0.

Jones, Dayton L., William M. Folkner, Robert A. Jacobson, Christopher S. Jacobs, Jonathan Romney, and Vivek Dhawan (2020), "Very Long Baseline Array Astrometry of Cassini: The Final Epochs and an Improved Orbit of Saturn." *Astron. J.*, 159, 72 doi: 10.3847/1538-3881/ab5f5d.

Kikuchi, Fuyuhiko, Yusuke Kono, Makoto Yoshikawa, Mamoru Sekido, Masafumi Ohnishi, Yasuhiro Murata, Jinsong Ping, Qinghui Liu, Koji Matsumoto, Kazuyoshi Asari, Seiitsu Tsuruta, Hideo Hanada, and Nobuyuki Kawano (2004), "VLBI observation of narrow bandwidth signals from the spacecraft." *Earth, Planets and Space*, 56, 1041–1047 doi: 10.1186/bf03352546.

Klopotek, Grzegorz, Thomas Hobiger, Ruediger Haas, Frederic Jaron, Laura La Porta, Axel Nothnagel, Zhongkai Zhang, Songtao Han, Alexander Neidhardt, and Christian Ploetz (2019), "Position determination of the chan-e3 lander with geodetic vlbi." *Earth, Planets and Space*, 71, 23 doi: 10.1186/s40623-019-1001-2.

Kopeikin, Sergei M. and Gerhard Schäfer (1999), "Lorentz covariant theory of light propagation in gravitational fields of arbitrary-moving bodies." *Physical Review D*, 60 doi: 10.1103/physrevd.60.124002.

Kovalev, Y. Y., L. Petrov, E. B. Fomalont, and D. Gordon (2007), "The Fifth VLBA Calibrator Survey: VCS5." *Astron. J.*, 133, 1236–1242 doi: 10.1086/511157.

Martí-Vidal, I., E. Ros, M. A. Pérez-Torres, J. C. Guirado, S. Jiménez-Monferrer, and J. M. Marcaide (2010), "Coherence loss in phase-referenced VLBI observations." *Astron. & Astrophys.*, 515, A53 doi: 10.1051/0004-6361/201014203.

Matsumoto, Koji, Ryuhei Yamada, Fuyuhiko Kikuchi, Shunichi Kamata, Yoshiaki Ishihara, Takahiro Iwata, Hideo Hanada, and Sho Sasaki (2015), "Internal structure of the moon inferred from apollo seismic data and selenodetic data from GRAIL and LLR." *Geophysical Research Letters*, 42, 7351–7358 doi: 10.1002/2015gl065335.

Matsuyama, Isamu, Francis Nimmo, James T. Keane, Ngai H. Chan, G. Jeffrey Taylor, Mark A. Wieczorek, Walter S. Kiefer, and James G. Williams (2016), "GRAIL, LLR, and LOLA constraints on the interior structure of the moon." *Geophysical Research Letters*, 43, 8365–8375 doi: 10.1002/2016gl069952.

Meyer, Jennifer and Jack Wisdom (2011), "Precession of the lunar core." *Icarus*, 211, 921–924 doi: 10.1016/j.icarus.2010.09.016.

Murphy, T W (2013), "Lunar laser ranging: the millimeter challenge." *Reports on Progress in Physics*, 76, 076901 doi: 10.1088/0034-4885/76/7/076901.

Murphy, T W, E G Adelberger, J B R Battat, C D Hoyle, N H Johnson, R J McMillan, C W Stubbs, and H E Swanson (2012), "APOLLO: millimeter lunar laser ranging." *Classical and Quantum Gravity*, 29, 184005 doi: 10.1088/0264-9381/29/18/184005.

Park, Ryan S., William M. Folkner, Dayton L. Jones, James S. Border, Alexander S. Konopliv, Tomas J. Martin-Mur, Vivek Dhawan, Ed Fomalont, and Jonathan D. Romney (2015), "Very Long Baseline Array Astrometric Observations of Mars Orbiters." *Astron. J.*, 150, 121 doi: 10.1088/0004-6256/150/4/121.

Pavlov, Dmitry (2020), "Role of lunar laser ranging in realization of terrestrial, lunar, and ephemeris reference frames." *Journal of Geodesy*, 94, 5 doi: 10.1007/s00190-019-01333-y.

Pavlov, Dmitry A., James G. Williams, and Vladimir V. Suvorkin (2016), "Determining parameters of moon's orbital and rotational motion from LLR observations using GRAIL and IERS-recommended models." *Celestial Mechanics and Dynamical Astronomy*, 126, 61–88 doi: 10.1007/s10569-016-9712-1.

Petrov, L. (2011), "The Catalog of Positions of Optically Bright Extragalactic Radio Sources OBRS-1." *Astron. J.*, 142, 105 doi: 10.1088/0004-6256/142/4/105.

Petrov, L. (2012), "The EVN Galactic Plane Survey - EGaPS." *Mon. Not. Roy. Astr. Soc.*, 419, 1097–1106 doi: 10.1111/j.1365-2966.2011.19765.x.

Petrov, L. (2013), "The Catalog of Positions of Optically Bright Extragalactic Radio Sources OBRS-2." *Astron. J.*, 146, 5 doi: 10.1088/0004-6256/146/1/5.

Petrov, L., Y. Y. Kovalev, E. B. Fomalont, and D. Gordon (2005), "The Third VLBA Calibrator Survey: VCS3." *Astron. J.*, 129, 1163–1170 doi: 10.1086/426920.

Petrov, L., Y. Y. Kovalev, E. B. Fomalont, and D. Gordon (2006), "The Fourth VLBA Calibrator Survey: VCS4." *Astron. J.*, 131, 1872–1879 doi: 10.1086/499947.

Petrov, L., Y. Y. Kovalev, E. B. Fomalont, and D. Gordon (2008), "The Sixth VLBA Calibrator Survey: VCS6." *Astron. J.*, 136, 580–585 doi: 10.1088/0004-6256/136/2/580.

Petrov, L., Y. Y. Kovalev, E. B. Fomalont, and D. Gordon (2011a), "The Very Long Baseline Array Galactic Plane Survey–VGaPS." *Astron. J.*, 142, 35 doi: 10.1088/0004-6256/142/2/35.

Petrov, L., C. Phillips, A. Bertarini, T. Murphy, and E. M. Sadler (2011b), "The LBA Calibrator Survey of southern compact extragalactic radio sources - LCS1." *Mon. Not. Roy. Astr. Soc.*, 414, 2528–2539 doi: 10.1111/j.1365-2966.2011.18570.x.

Petrov, L. and G. B. Taylor (2011), "Precise Absolute Astrometry from the VLBA Imaging and Polarimetry Survey at 5 GHz." *Astron. J.*, 142, 89 doi: 10.1088/0004-6256/142/3/89.

Petrov, Leonid (2021), "The Wide-field VLBA Calibrator Survey: WFCS." *Astron. J.*, 161, 14 doi: 10.3847/1538-3881/abc4e1.

Petrov, Leonid, Alet de Witt, Elaine M. Sadler, Chris Phillips, and Shinji Horiuchi (2019), "The Second LBA Calibrator Survey of southern compact extragalactic radio sources - LCS2." *Mon. Not. Roy. Astr. Soc.*, 485, 88–101 doi: 10.1093/mnras/stz242.

Popkov, Alexander V., Yuri Y. Kovalev, Leonid Y. Petrov, and Yuri A. Kovalev (2020), "Parsec-scale properties of steep and flat spectrum extragalactic radio sources from a VLBA survey of a complete north polar cap sample." *arXiv e-prints*, arXiv:2008.06803.

Schinzel, F. K., L. Petrov, G. B. Taylor, and P. G. Edwards (2017), "Radio Follow-up on All Unassociated Gamma-Ray Sources from the Third Fermi Large Area Telescope Source Catalog." *Astrophys. J.*, 838, 139 doi: 10.3847/1538-4357/aa6439.

Schinzel, F. K., L. Petrov, G. B. Taylor, E. K. Mahony, P. G. Edwards, and Y. Y. Kovalev (2015), "New Associations of Gamma-Ray Sources from the Fermi Second Source Catalog." *Astrophys. J. Suppl. Ser.*, 217, 4 doi: 10.1088/0067-0049/217/1/4.

Shu, F., L. Petrov, W. Jiang, B. Xia, T. Jiang, Y. Cui, K. Takefuji, J. McCallum, J. Lovell, S.-o. Yi, L. Hao, W. Yang, H. Zhang, Z. Chen, and J. Li (2017), "VLBI Ecliptic Plane Survey: VEPS-1." *Astrophys. J. Suppl. Ser.*, 230, 13 doi: 10.3847/1538-4365/aa71a3.

Sun, Jing, Geshi Tang, Fengchun Shu, Xie Li, Shushi Liu, Jianfeng Cao, Andreas Hellerschmied, Johannes Böhm, Lucia McCallum, Jamie McCallum, Jim Lovell, Rüdiger Haas, Alexander Neidhardt, Weitao Lu, Songtao Han, Tianpeng Ren, Lue Chen, Mei Wang, and Jinsong Ping (2018), "VLBI observations to the APOD satellite." *Advances in Space Research*, 61, 823–829 doi: 10.1016/j.asr.2017.10.046.

Thompson, A. R., J. M. Moran, and G. W. Swenson, Jr. (2017), *Interferometry and Synthesis in Radio Astronomy, 3rd Edition*. Springer.

Turyshev, Slava G., James G. Williams, William M. Folkner, Gary M. Gutt, Richard T. Baran, Randall C. Hein, Ruwan P. Somawardhana, John A. Lipa, and Suwen Wang (2012), "Corner-cube retro-reflector instrument for advanced lunar laser ranging." *Experimental Astronomy*, 36, 105–135 doi: 10.1007/s10686-012-9324-z.

Williams, James G. and Dale. H. Boggs (2015), "Tides on the moon: Theory and determination of dissipation." *Journal of Geophysical Research: Planets*, 120, 689–724 doi: 10.1002/2014je004755.

Williams, James G. and Dale H. Boggs (2016), "Secular tidal changes in lunar orbit and earth rotation." *Celestial Mechanics and Dynamical Astronomy*, 126, 89–129 doi: 10.1007/s10569-016-9702-3.

Williams, James G, Slava G Turyshev, and Dale H Boggs (2012), "Lunar laser ranging tests of the equivalence principle." *Classical and Quantum Gravity*, 29, 184004 doi: 10.1088/0264-9381/29/18/184004.

Williams, James G, Slava G Turyshev, and Dale H Boggs (2014), "The past and present earth-moon system: the speed of light stays steady as tides evolve." *Planetary Science*, 3 doi: 10.1186/s13535-014-0002-5.

9 Biographical Sketches

Leonid Petrov (PI)

Present position:

Geophysicist at NASA GSFC in Geodesy & Geophysics Laboratory at NASA GSFC, VLBI Lead Scientist.

Professional experience:

Since 1988 Leonid Petrov has been working in data analysis of space geodesy and remote sensing data, development of data processing algorithms with the highest accuracy, systems and tools aimed to improvement of the terrestrial and celestial reference frames and Earth orientation parameters. He has developed algorithms and implemented them into software for VLBI scheduling, VLBI post-correlation processing based on cross-spectrum, for computation of theoretical VLBI delay, and for geodetic and astrometric VLBI data analysis based on group delays. He has processed all publicly available VLBI observations suitable for astrometry and geodesy.

Leonid Petrov NASA worked at Goddard Earth Sciences Data and Information Services Center for support of the infrastructure for visualization, analyzing, and access of vast amounts of Earth science remote sensing data. During his carrier has has developed over one million line of code for various scientific applications.

Leonid Petrov has been working on development of advanced methods for processing space geodesy, remote sensing data, and numerical models. He has been working on development and maintenance of the pipeline for prepossessing, analysis, and interpretation of VLBI geodetic experiments that was adopted by the International VLBI Service. He also worked on development and maintenance of the International Mass Loading Service, the International Path Delay Service, the Atmospheric Angular Momentum Service, and the Network Earth Rotation Service.

Management experience:

Managed twenty seven projects under various astronomy programs at the National Radio Astronomy Observatory, the European VLBI Network, Australian National Telescope Facility, East Asian VLBI Network, National Astronomical Observatory of Japan, Korea Astronomy and Space Science.

Managed seven projects under NASA Earth Surface and Interior program and one project under NASA Global Navigation Satellite System Remote Sensing Science Team as a principal investigator.

Education:

Ph.D. of Russian Academy of Sciences, 1995, Astronomy
M.S. of Leningrad National University, 1988, Astronomy

Selected publications

1. **Petrov, L.**, "The wide-field VLBA calibrator survey – WFCS", (2021), Astronomical Journal, 161(1), 15 (25pp). doi: 10.3847/1538-3881/abc4e1

2. **Petrov, L.**, (2016), "The International Mass Loading Service", International Association of Geodesy Symposia, Springer, vol 146, 79–83. doi: 10.1007/1345_2015_218

3. **Petrov, L.**, T. Natusch, S. Weston, J. McCallum, S. Ellingsen, S. Gulyaev, (2015). "First scientific VLBI observations using New Zealand 30 meter radio telescope WARK30M", Publications of the Astronomical Society of the Pacific, 127, 516–522

4. **Petrov, L.**, (2015), Modeling of path delay in the neutral atmosphere: a paradigm shift, to appear in the Proceedings of the 12th European VLBI Network Symposium and Users Meeting, 7-10 October 2014 Cagliari, Italy http://arxiv.org/abs/1502.06678

5. P. Sarti, C. Abbondanza, **L. Petrov**, M. Negusini, (2010) "Effect of antenna gravity deformations on VLBI estimates of site positions", Jour. of Geodesy, DOI: 10.1007/s00190-010-0410-6.

6. **Petrov, L.**, D. Gordon, J. Gipson, D. MacMillan, C. Ma, E. Fomalont, R. C. Walker, C. Carabajal, (2009) "Precise geodesy with the Very Long Baseline Array", Journal of Geodesy, vol. 83(9), 859.

7. **Petrov, L.**, (2007) "The empirical Earth rotation model from VLBI observations", Astronomy and Astrophysics, vol. 467, p. 359.

8. **Petrov, L.**, C. Phillips, A. Bertarini, A. Deller, S. Pogrebenko, A. Mujunen, (2009) "The use of the Long Baseline Array in Australia for precise geodesy and absolute astrometry", Publications of the Astronomical Society of Australia, 26(1), 75-84.

9. **Petrov, L.**, J.-P. Boy, (2004) "Study of the atmospheric pressure loading signal in VLBI observations", Journal of Geophysical Research, 10.1029/2003JB002500, vol. 109, No. B03405.

10. **Petrov, L.**, C. Ma, (2003) "Study of harmonic site position variations determined by VLBI", Journal of Geophysical Research, vol. 108, No. B4, 2190.

11. **Petrov, L.**, O. Volvach, N. Nesterov, "Measurements of horizontal motion of the station Simeiz using VLBI", (2001) Kinematic and Physics of Celestial Bodies, Vol. 17, N5, p. 424–436.

There are 59 peer reviewed works with a total of 2347 citations. Hirsch index 26.

10 Summary of Work Effort

g

11 Current and pending support

Current and pending support — Principle Investigator Leonid Petrov

12 Budget Justification (narrative) including facilities and equipment

13 Budget Details (redacted)